Int. J. Electrochem. Sci., 17 **(2022)** Article Number: 221039, doi: 10.20964/2022.10.40

International Journal of
ELECTROCHEMICAL
SCIENCE
www.electrochemsci.org

Short Communication

Effect of Friction Stir Weld Parameters on Mechanical and Corrosion Performances of 5A06 Aluminum Alloy Plate Joints in 3.5 wt% NaCl solution

Yanyan Feng[1,*],*Fan Yang*[2], *Yan Bi*[1]

[1] College of Mechanical Engineering, Tianjin Sino-German University of Applied Sciences, Tianjin 300350, China
[2] Offshore Oil Engineering Co., Ltd, Tianjin 300350, China
[*]E-mail: fyy.yang@foxmail.com

Received: 12 July 2022 / *Accepted:* 12 August 2022 / *Published:* 10 September 2022

The conventional fusion welding process is not suitable for welding aluminium alloys because welding defects such as secondary brittle phase, porosity, and cracks can easily form during the solidification process of the aluminium alloy. Friction stir welding (FSW) is a new solid-state welding process suitable for joining similar and dissimilar materials, especially aluminium alloys. The study of the FSW parameters and their effects on weld quality and joint performance is very important to develop a comprehensive understanding of the fundamentals of microstructural evolution during FSW treatment. The effects of FSW parameters, such as rotation speeds and welding speed, on the microstructure and mechanical behaviour of FSW-welded 5A06 aluminium alloy joints were investigated. The results show that the rotation speed is the key factor that can play an important role in determining the defects and homogeneity of the weld microstructure. The study of the mechanical properties and electrochemical corrosion performances on the FSW joint shows that the fine and uniform weld microstructure formed at a rotation speed of 900 rpm has positive potential, lower corrosion current density and higher tensile strength than the FSW joint with 300 and 600 rpm rotation speed. The FSW parameters play an important role in determining the corrosion and mechanical behaviours and microstructure homogeneity.

Keywords: Friction Stir Welded; Slow strain rate stress; Mechanical properties; Electrochemical corrosion.

1. INTRODUCTION

Aluminium alloys are characterized by low price, low density and high strength, excellent corrosion resistance, and ease of manufacture. Aluminium alloy 5A06 , a type of high-strength 5xxx Al-Mg alloy, is widely used in marine, automotive, and aerospace applications due to its above-mentioned properties [1]. Welding is an important means of reducing the manufacturing cost of aluminium alloy joints. However, the conventional fusion welding processes are not suitable for welding aluminium

alloys. This is due to the fact that during the solidification process, there is always the formation of secondary phases, porosity and cracks [2], as well as high residual stresses in the welding area. The above-mentioned problems of aluminium alloy welded joints are difficult to avoid with the conventional fusion welding processes, e.g., pure laser welding. Compared to fusion welding, FSW is a solid-state connection technology invented in 1991 by The Welding Institute (TWI) of the United Kingdom, and has proven to be particularly suitable for the joining of aluminium alloys [2]. FSW is a hot-shear joining process [3, 4] in which a rotating tool with a shoulder and terminating in a threaded pin, moves along the butting surfaces of two rigidly clamped plates placed on a backing plate [5].

In addition, the FSW process is considered as the most important development in the field of metal connection in recent years. Compared with the conventional welding process, FSW has the advantages of energy saving, environmental protection and great universality. Originally, it was applied to aluminium alloys [6, 7]. After more than 30 years of development, the FSW process has covered magnesium alloys [5, 8], copper [9-11], titanium alloys [12-16], lithium alloys [17, 18], thermoplastic materials, etc [19]. In the FSW process, the material in the weld zone is subject to strong thermos-mechanical excursions [20], which lead to recrystallization and recovery processes. In the FSW process, the heat and mass transfer depend on the material properties and the welding variables, including tool rotation and welding speed and its geometry. The rotation of the cutter causes the materials to move around the rotary pin and mix through plastic flow. Friction between the cutter and the workpiece is the main cause of heat generation. The microstructure composition and the development of the FSW joint from the parent metal can affect the mechanical properties, including the hardness profile, tensile properties as well as fracture properties of the welding joint. Studies of FSW weld microstructures, and the dynamic recrystallization mechanism have shown that the microstructure and mechanical properties mainly depend on the relative plastic deformation and heat distribution in the joint area [2]. The selected FSW parameters, e.g., rotational speed and travel speed, have a significant effect on the microstructure homogeneity, mechanical properties, corrosion, and the residual stress distribution in the weld of the FSW joint [6]. Therefore, it is necessary to optimize the FSW parameters in order to improve the weld quality and avoid the generation of microscopic defects.

In this study, a preliminary investigation on the effect of rotational speed during FSW joining was conducted and a comprehensive analysis was also extended. Different rotating speeds were optimized on 5A06 aluminium alloy sheets to homogenize the weld microstructure and to improve the mechanical and corrosion performances. The relationship between joint microstructures and their corresponding performances was studied to find out the optimal parameters for the FSW of the 5A06 aluminium alloy.

2. EXPERIMENTAL

2.1. Materials

The base material used in this study is a 5A06 aluminium alloy sheet with a size of 50 × 300 × 6 mm. A total of 6 plates were connected to obtain 3 joints. Table 1 lists the chemical composition of the plates. Before friction stir welding, the surface of the plate is mechanically polished, and then wiped with ethanol to remove the surface oxides and impurities.

Table 1. Metallurgical composition of 5A06 aluminium alloy (wt %).

Si	Mn	Fe	Mg	Zn	Al
0.4	0.5-0.8	0.4	5.2-6.8	0.2	Bal.

2.2 Friction stir welding process

The friction stir welding equipment, welding process and simple geometry of the stir tool are shown in Fig. 1. The FSW stir tool is made of H13 steel with a shoulder diameter of 18 mm and a conical pin 5.7 mm in length, while the root of the pin has a diameter of 6 mm. As shown in Fig. 1b, the rotation speed of the FSW stir tool is rotational speed ω, and the moving speed of the FSW stir tool along the weld direction is the welding speed V. To investigate the effects of tool rotational, we chose three different rotation speeds for friction stir welding. The three samples with different rotating speeds are named F1, F2 and F3, respectively. The parameters are listed in Table 2. The mild steel fixture is used to fix the plate on the workbench for friction stir welding. The plates should cool down for 20 min after the FSW process.

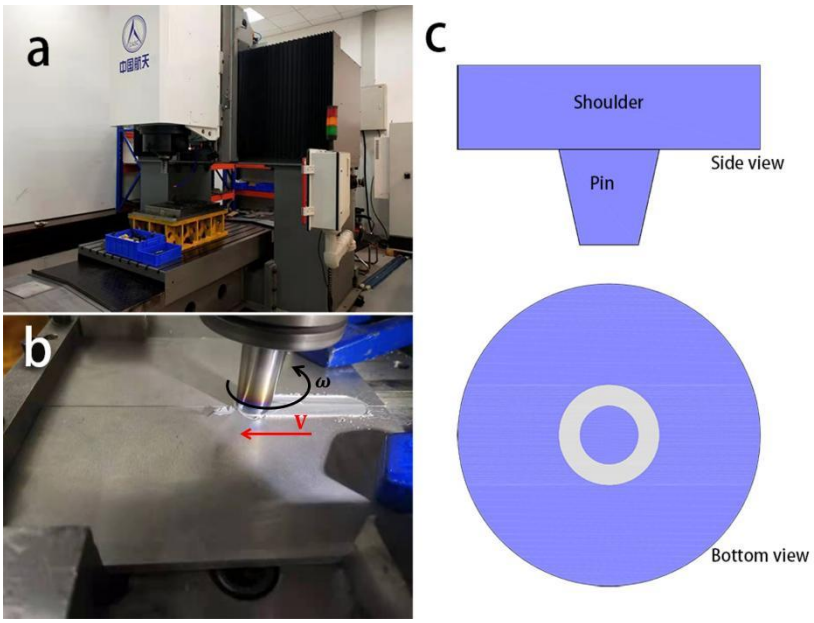

Figure 1. (a) Photograph of the FSW equipment. (b) the FSW process. (c) simple geometry of the stir tool.

Table 2. Processing parameters of the FSW

Sample name	Rotational speed ω (rpm)	Welding speed V (mm/min)
F1	300	80
F2	600	80
F3	900	80

2.3 Microstructure

The three samples after FSW welding are sliced by electrical discharge machining and polished with 100-2000# SiC sandpaper. Then these sliced samples were etched with Keller's corrosion reagent which contained 2.5 ml of nitric acid, 1.5 ml of hydrochloric acid, 1 ml of hydrofluoric acid, and 95ml of distilled water. In this study, JSM-7800F thermal field emission scanning electron microscope of the JEOL company was used to observe the fracture morphology of the sample after slow tensile corrosion, and the corrosion products were analysed by energy spectrum. The Axio observer inverted biological microscope from Zeiss company was used to observe the optical metallography.

2.4 SSRT testing

SSRT experiments were performed in the test kettle inside the Bairoe YYF-50 stress corrosion testing machine with a test solution at 25 °C under a strain rate of $1 \times 10^{-6} s^{-1}$. For comparison, samples were tested in air and in a corrosion solution, respectively, using the same welding procedure. The corrosion test solution consisted of 3.5 wt % NaCl.

2.5 Electrochemical testing

To analyse the overall electrochemical corrosion performance of friction stir welded joints and their role in stress corrosion, the electrochemical behaviour of friction stir welded joints at different rotational speeds in NaCl solution was investigated by a potentiodynamic polarization curve test. The electrochemical corrosion test solution consisted of 3.5 wt % NaCl. The tests were performed using a CH Instruments 660E electrochemical measurement unit equipped with a three-electrode cell system. The electrochemical sample of the friction stir welding joint is the working electrode, the saturated calomel electrode is the reference electrode, and the platinum electrode is the counter electrode. The electrochemical samples were obtained by Wire cut Electrical Discharge Machining. The size of the electrochemical sample is 12 × 12 × 4 mm. The sample is encapsulated with epoxy resin, and a test area of 12 mm^2 is reserved on the surface. Before testing, all these samples were polished with 800-2000# SiC paper, then cleaned with deionized water and alcohol, and dried for readiness. The scanning rate of the potentiodynamic polarization curve was 1 mV/s and the range was from −1.7 to -0.2 V. All electrochemical tests were performed at room temperature and normal pressure (25 ℃, 0.1 MPa).

3. RESULTS AND DISCUSSION

3.1 Macroscopic morphology

As can be seen in Fig. 2, no obvious fusion defects were found on the surfaces of the three samples. As can be seen in Fig. 3, the friction stir welded joint consists of the weld nugget zone (WNZ), thermo-mechanical affected zone (TMAZ), the heat affected zone (HAZ) and the base metal (BM) which are clearly marked. The width of the WNZ increases from 7.6 to 11.1 mm when the rotation speed is increased from 300 to 900 rpm. This is because the area of the recrystallized zone increases when the

temperature rises to 400-550 ^{o}C [21] while the tool rotates at a high speed [3]. Fig. 5 shows the details of welded joints. Fig. 5a is the base metal of 5A06 aluminium alloy. The macrostructure of the thermo-mechanically affected area, corresponding to the RS and AS of the weld, is shown in Fig. 5 (c) and (d), respectively. In Fig. 5e, "onion rings" can be seen in the WNZ region of the F2 sample. The "onion ring" is a consequence of the way a threaded tool deposits material from the front to the back of the weld [22]. Fig.5f shows the void defects in the WNZ region of the F1 sample. Void defects usually occur on the forward side of FSW joint, which is due to insufficient material flow on the advancing side [20, 23].

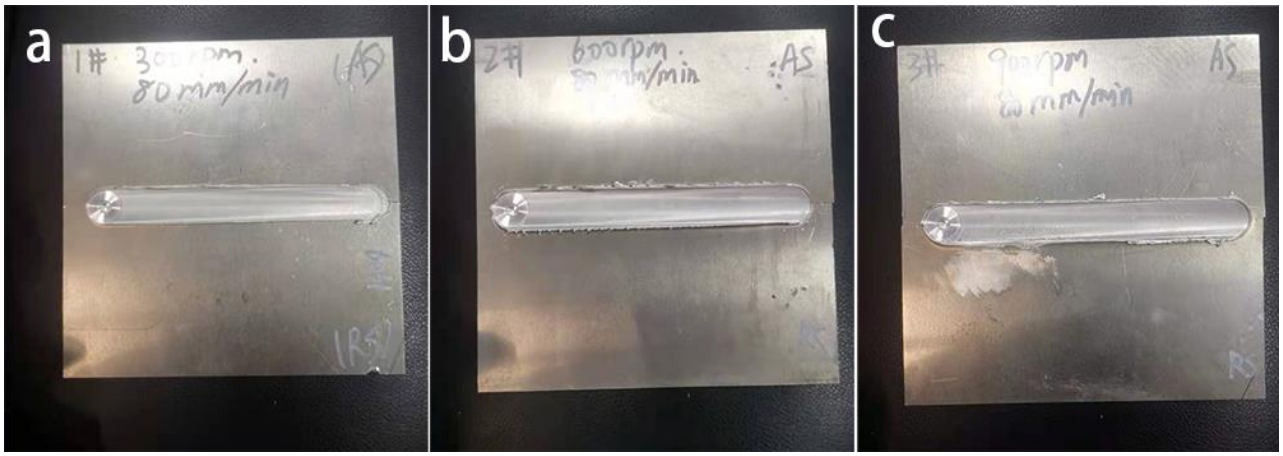

Figure 2. Digitial photos of FSW samples with different rotation speeds. (a) 300 rpm, (b) 600 rpm, (c) 900 rpm.

Figure 3. Metallurgical zones of friction stir welded joint with a rotating speed of 900 rpm.

In the optical micrographs of the three samples (Fig. 4), the typical S-curves can be seen, showing that there are residues of the base metal grain boundary in the WNZ region, which were formed due to the strong plastic deformation under the action of the stirring pin. The frictional heat generated during FSW and the strong plastic deformation caused by the stirring needle led to microstructural changes such as recrystallization and grain growth of the joint. The flow of the metal materials around the stirring needle varies due to the different rotation speeds. For sample F1, at a low welding speed of 300 rpm, the metal flow around the mixing head was insufficient, which may lead to the formation of a micro-void. When the rotation speed is 300 rpm, the plastic deformation ability of the base metal in WNZ region is insufficient to refill the micro-void. When the rotation speed was increased to 900 rpm, the base metal could sufficiently fill the micro-void defect. Guan analysed the typical force signal of friction stir

welding and its response to welding defects. They found that the size of void defects gradually decreased as the rotating speed increased [24].

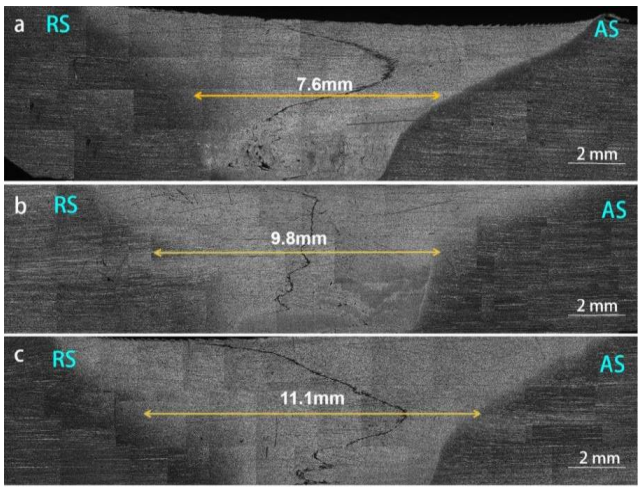

Figure 4. Optical micrographs of three samples with different rotation speeds: (a) 300 rpm, (b) 600 rpm, (c) 900 rpm.

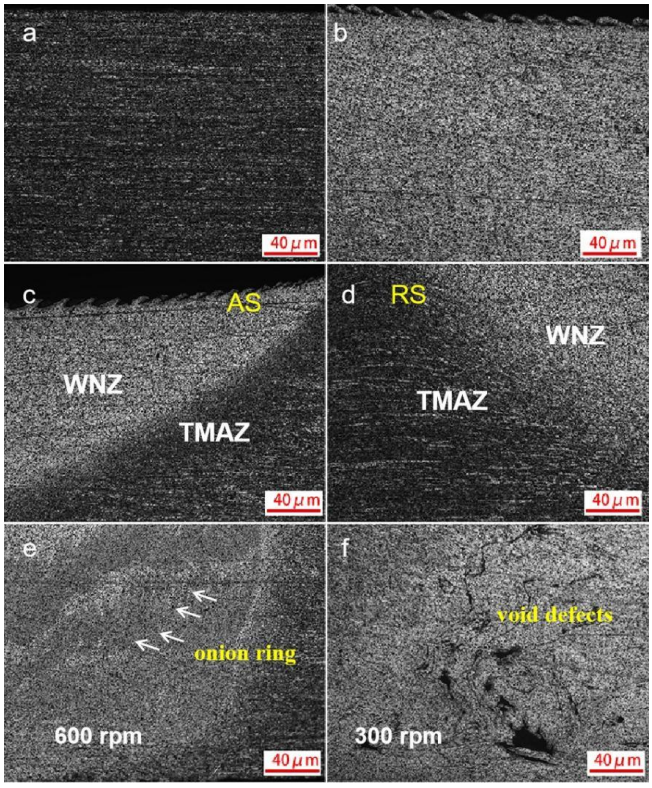

Figure 5. Optical micrographs of different parts of the FSW joint: (a) BM of F1 with a rotation speed of 300 rpm, (b) WNZ of F1 with a rotation speed of 300 rpm,(c)TMAZ on the advancing side of F1 with a rotation speed of 300 rpm, (d) TMAZ on the retreating side of F1 with a rotation speed of 300 rpm, (e) root of WNZ in F2 with a rotation speed of 600 rpm and (f) root of the WNZ in F1 with a rotation speed of 300 rpm.

3.2 SSRT Properties

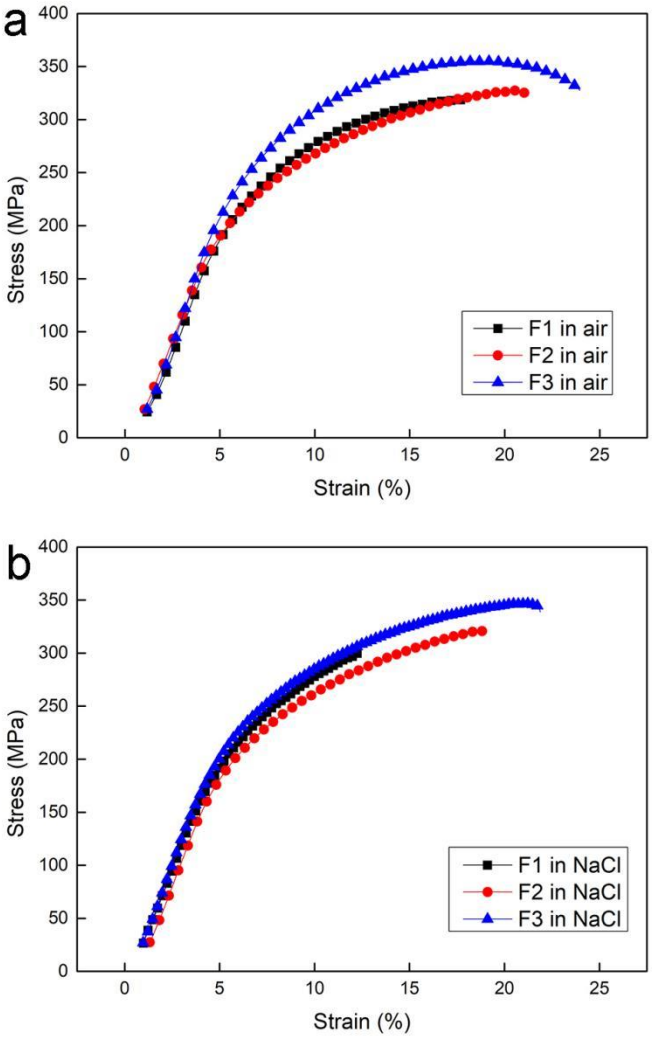

Figure 6. The stress-strain curve in different test environments. (a) in air and (b) in 3.5 wt % NaCl.

Table 3. Summary of tensile properties under different test conditions with fusion welding.

Sample name	Test environment	YS(MPa)	UTS(MPa)	EI.%
F1	air	176	325	10.3
	NaCl	166	301	5.9
F2	air	177	327	13.9
	NaCl	166	322	11.6
F3	air	197	352	19.1
	NaCl	176	347	14.7

The SSRT stress-strain curves of the three samples are shown in Fig.6, and the specific values of mechanical properties are listed in Table 3. The mechanical properties of sample F1 are overall worse than those of the other two groups when the data is compared. In conjunction with Fig.5f, sample F1

shows the worst mechanical properties among the three samples, which is due to the void defects formation at the joint at a rotational speed of 300 rpm. Low rotational speed easily leads to kissing bonds and tunnel defects [21, 25].

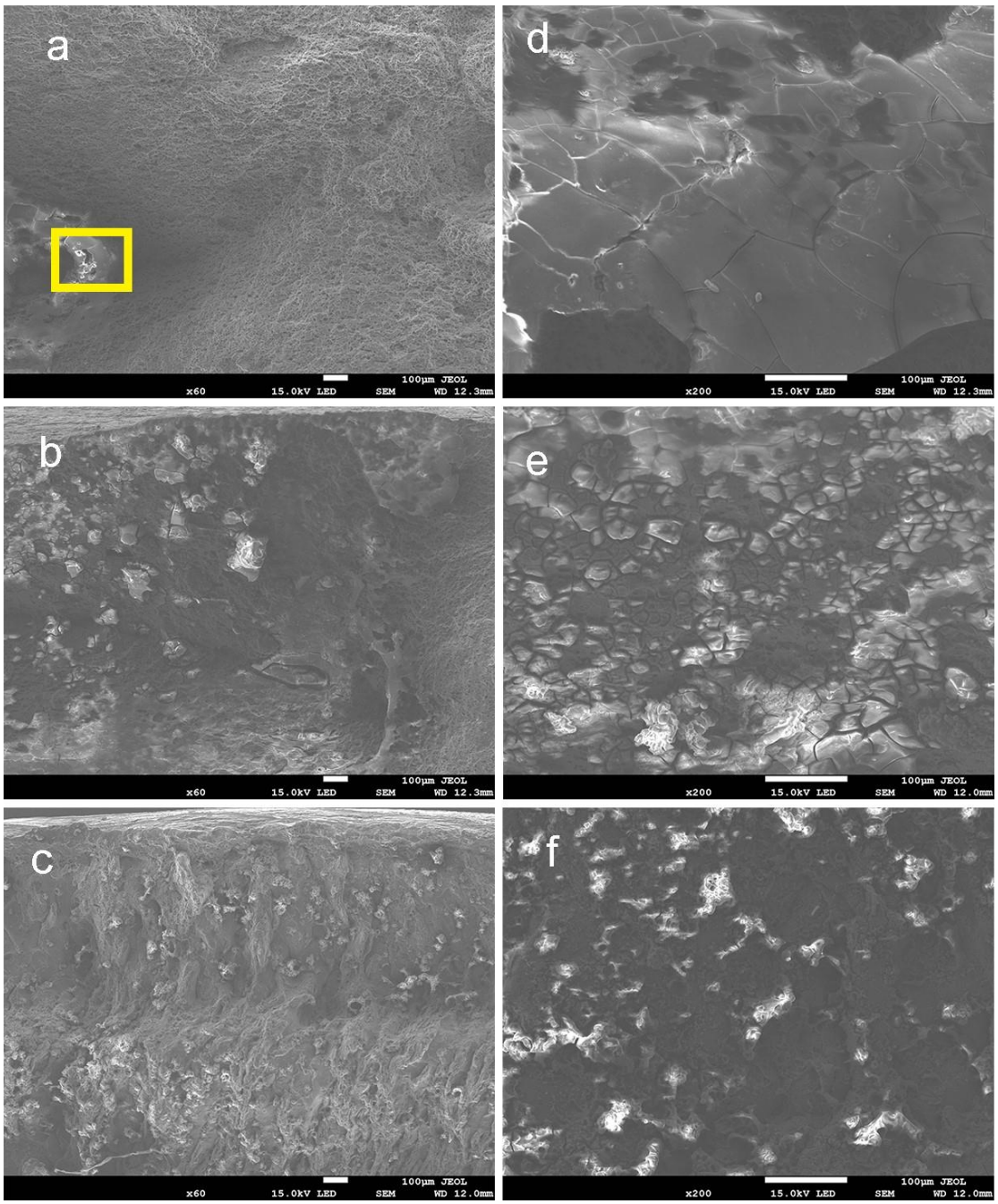

Figure 7. SEM images of SSRT fractures for samples F1, F2 and F3 in 3.5 wt % NaCl: (a)-(c). And (d)–(f) are magnified images marked by a yellow rectangle in (a)–(c).

Under corrosive 3.5 wt % NaCl solution, the plasticity loss of F2 is 13 % and that of F3 is 23 %. As shown in Table 3, the ultimate/yield strength of F3 is better than that of F1 and F2 in both non-corrosive and corrosive environments. The yield strength values of the F3 sample are 197 MPa and 176 MPa in air and 3.5 wt % NaCl respectively. The ultimate tensile strength of the F3 sample is 352 MPa

and 347 MPa in air and 3.5 wt% NaCl, respectively. The breaking elongation of the F3 sample under corrosive conditions is about 15 %.

Fig.6 shows the fracture morphology of the three samples after the corrosive treatments. The fracture initiation point of the F1 sample is marked by the yellow frame as shown in Fig.6a. As can be seen in Fig.6d, the fracture surface is flush and the initial crack is characterized by a brittle fracture, which then develops into a plastic fracture around the fracture initiation site.

It can be concluded that the crack was initiated due to the void defect, and the non-uniform fusion of the metals around the defect leads to the grain boundary opening under stress. The in-situ cell was formed when the corroding NaCl solution entered the gap of the grain boundary and led to the crack propagation. The crack propagates gradually and leads to ductile fracture across the sample sub-surface, as shown in Fig.7a. Fig.8 shows the EDX spectrum of 5A06 aluminium alloy after NaCl corrosion.

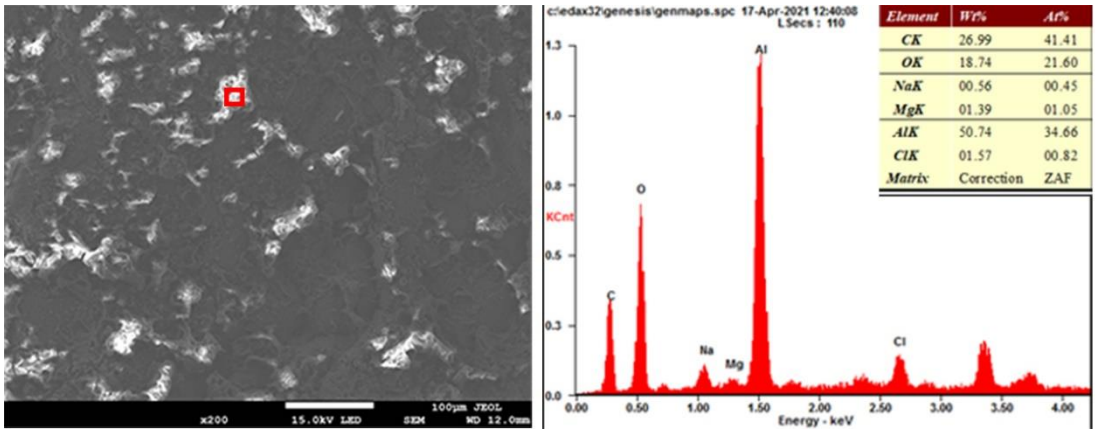

Figure 8. EDX spectrum of 5A06 aluminium alloy after NaCl corrosion.

3.3 Electrochemical analysis

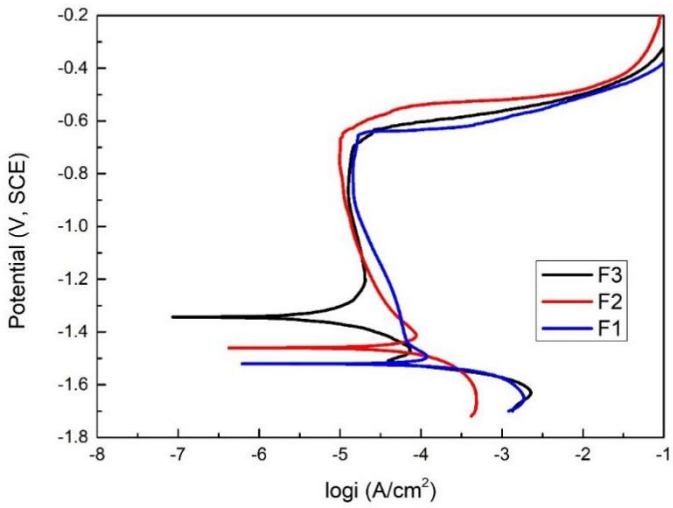

Figure 9. Potentiodynamic polarization curves of three FSW joints in 3.5% NaCl

Table 4. Table 4 Tafel parameters of three samples in 3.5 wt% NaCl solution

Sample name	Corrosion potential (E_{cor} [V])	Corrosion current (I_{cor} [A/cm^2])
F1	-1.521	3.838e-004
F2	-1.460	2.509e-004
F3	-1.344	4.302e-005

The corrosion behaviour of FSW 5A06 aluminium alloy was studied using standard polarisation measurements. Tafel polarisation tests were conducted to determine the corrosion resistance in 3.5 wt% NaCl solution (pH = 7), and the results were used to evaluate the influence of rotational speed on corrosion resistance of joints. Tafel curves of the three samples (F1, F2, and F3) are shown in Fig. 9, and the corresponding corrosion potential (E_{cor}) and corrosion current (I_{cor}) values are summarised in Table 4. These results demonstrate that corrosion resistance of joints increases with increasing rotational speed; this is because of the reduction of the second phase and defects in the structure. The high rotational speed of 900 rpm can lead to a uniform joint microstructure without any other second phases and defects during the FSW process. The defects formed in friction welding typically exhibit high chemical activity, and the potential is lower than the matrix, thus forming a galvanic cell with the matrix. The defect is the anode, and the corrosion is accelerated, resulting in a decrease in both the self-corrosion potential and current density of the material [26]. With an increase in the friction welding rotational speed, the increasing deformation temperature enhances the homogeneity of the recrystallised microstructure. The microstructure of the WNZ is uniform, and the micro-void defects can be refilled; thus, the defects in the material are significantly reduced, and the corrosion resistance of the material is improved.

4. CONCLUSION

The three FSW 5A06 aluminium alloy samples were produced at different rotational speeds of 300, 600, and 900 rpm. The microstructures of the three samples show s-shaped curves, indicating that residue is present in the original interface of the Al-based alloy. A void defect can be seen in the SNZ of the F1 sample. There was insufficient metal flow in the SNZ of the F2 sample, resulting in an uneven joint. The slow strain rate tensile tests in air resulted in yield strengths of 176 and 177 MPa for F1 and F2, respectively, and the yield strength of F3 was 197 MPa, which is 119 % and 112 % of the other two samples. At high rotational speeds, there is a high heat accumulation and an improved degree of mixing, which increases the yield strength and ultimate tensile strength. The corrosion resistance of the three samples was tested under 3.5 wt% NaCl corrosion solution. The values of the corrosion potential Ecor demonstrate that the corrosion resistance of the joints increases with an increase in the rotational speed. The electrochemical results indicate that the presence of micro-void defects significantly weakens the corrosion resistance of the FSW samples. In addition, from the fracture, it was found that the corrosive liquid easily penetrates into the void defect to form a galvanic cell, resulting in brittle fracture characteristics at the origin of the fracture crack, and the elongation at break was only 5.9 % in Sample F1. The elongation at break of F3 was 14.7 %, and there were dimples on the fracture surface, which is characteristic of ductile fracture.

ACKNOWLEDGEMENTS
This work was supported by the National Natural Science Foundation of China (5187050926), and the Natural Science Foundation of Tianjin City (20YDTPJC01740).

References

1. Z. Wang, J. P. Oliveira, Z. Zeng, X. Bu, B. Peng and X. Shao, *Opt. Laser Technol.*, 111 (2019) 58.
2. N. Guo, Y. Fu, Y. Wang, Q. Meng and Y. Zhu, *Mater. Des.*, 113 (2017) 273.
3. R. S. Mishra and Z. Y. Ma,Mater. *Sci. Eng., R*, 50 (2005) 1.
4. E. Liverani, F. Zanini, L. Tonelli, S. Carmignato and A. Fortunato, *J. Manuf. Processes*, 71 (2021) 541.
5. L. H. Shah, N. Huda, S. Esmaeili, S. Walbridge and A. P. Gerlich, *Mater. Lett.*, 275 (2020) 128098.
6. U. K. Singh and A. K. Dubey, *Proc. Inst. Mech. Eng., Part C: J. Mech. Eng. Sci.*, 235 (2021) 3554.
7. A. Shrivastava, M. Zinn, N. A. Duffie, N. J. Ferrier, C. B. Smith and F. E. Pfefferkorn, *J. Manuf. Processes*, 26 (2017) 113.
8. F. Tolun, *Kovove Mater.*, 60 (2022) 109.
9. J. Q. You, Y. Q. Zhao, C. L. Dong, Y. Y. Yi and Y. H. Su, *J. Mater. Eng. Perform.*, 30 (2021) 2751.
10. P. Q. Gao, Y. Zhang and K. P. Mehta, *Met. Mater. Int.*, 27 (2021, 3085.
11. Y. Y. Zuo, L. P. Kong, Z. L. Liu, Z. Lv and H. J. Wen, *Trans. Indian Inst. Met.*, 73 (2020) 2975.
12. J. Yan, M. A. Sutton and A. P. Reynolds, *Sci. Technol. Weld. Joining*, 10 (2005) 725.
13. M. Reimann, J. Goebel, T. M. Gartner and J. F. dos Santos, *J. Mater. Process. Technol.*, 245 (2017) 157.
14. A. A. Eliseev, S. V. Fortuna, A. I. Amirov, T. A. Kalashnikova, V. E. Rubtsov and E. A. Kolubaev, *Russ. Phys. J.*, 63 (2020) 467.
15. M. Yu, H. Zhao, Z. Jiang, Z. Zhang, F. Xu, L. Zhou and X. Song, *J. Mater. Sci. Eng*, 35 (2019) 1543.
16. J. P. Li, F. J. Cao and Y. F. Shen, *Metals*, 10 (2020) 940.
17. L. Shi, J. Chen, C. S. Wu and L. Fu, *Sci. Technol. Weld. Joining*, 26 (2021) 363.
18. Y. L. Ma, H. B. Xu, Z. Y. Liang and L. Liu, *Acta Metall. Sinica Engl.Lett.*, 33 (2020) 127.
19. R. Sandeep and N. Arivazhagan, *J. Braz. Soc. Mech. Sci. Eng.*, 43 (2021) 27.
20. T. Seidel and A. P. Reynolds, *Sci. Technol. Weld. Joining*, 8 (2003) 175.
21. M. Amatullah, M. Jan, M. Farooq, A. S. Zargar, A. Maqbool and N. Z. Khan, *Mater. Today:. Proc.*, 62 (2022) 245.
22. R. Nandan, T. DebRoy and H. K. D. H. Bhadeshia, *Prog. Mater Sci.*, 53 (2008) 980.
23. P. Prangnell and C. Heason, *Acta Mater.*, 53 (2005) 3179.
24. W. Guan, D. Li, L. Cui, D. Wang, S. Wu, S. Kang, J. Wang, L. Mao and X. Zheng, *J. Manuf. Processes*, 71 (2021) 1.
25. A. Goyal and R. K. Garg, *Int. J. Microstruct. Mater. Prop.*, 12 (2017) 79.
26. T. Majeed, Y. Mehta and A. Noor Siddiquee, *Mater. Today:. Proc.*, 62 (2022) 26.